

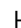
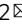


Realization of quasicrystalline quadrupole topological insulators in electrical circuits

Bo Lv^{1,7}, Rui Chen^{2,3,4,7}, Rujiang Li⁵ [✉], Chunying Guan¹, Bin Zhou², Guohua Dong¹, Chao Zhao¹, YiCheng Li¹, Ying Wang¹, Huibin Tao⁶ [✉], Jinhui Shi¹ [✉] & Dong-Hui Xu² [✉]

Quadrupole topological insulators are a new class of topological insulators with quantized quadrupole moments, which support protected gapless corner states. The experimental demonstrations of quadrupole-topological insulators were reported in a series of artificial materials, such as photonic crystals, acoustic crystals, and electrical circuits. In all these cases, the underlying structures have discrete translational symmetry and thus are periodic. Here we experimentally realize two-dimensional aperiodic-quasicrystalline quadrupole-topological insulators by constructing them in electrical circuits, and observe the spectrally and spatially localized corner modes. In measurement, the modes appear as topological boundary resonances in the corner impedance spectra. Additionally, we demonstrate the robustness of corner modes on the circuit. Our circuit design may be extended to study topological phases in higher-dimensional aperiodic structures.

¹Key Laboratory of In-Fiber Integrated Optics of Ministry of Education, College of Physics and Optoelectronic Engineering, Harbin Engineering University, Harbin, China. ²Department of Physics, Hubei University, Wuhan, China. ³Shenzhen Institute for Quantum Science and Engineering and Department of Physics, Southern University of Science and Technology (SUSTech), Shenzhen, China. ⁴School of Physics, Southeast University, Nanjing, China. ⁵Key Laboratory of Antennas and Microwave Technology, School of Electronic Engineering, Xidian University, Xi'an, China. ⁶School of Software Engineering, Xi'an Jiaotong University, Xi'an, China. ⁷These authors contributed equally Bo Lv, Rui Chen. [✉]email: rujiangli@xidian.edu.cn; coldfire_arm@126.com; shijinhui@hrbeu.edu.cn; donghuixu@hubu.edu.cn

Since the discovery of topological insulators (TIs), tremendous effort has been devoted to the search for exotic topological phases of matter^{1–10}. Recently, a novel class of exotic insulators with higher-order band topology, dubbed higher-order TIs (HOTIs), have been proposed^{11–26}. The fascinating characteristic of HOTIs is that d -dimensional n th-order TIs have $(d-n)$ -dimensional gapless boundary states^{11–16}. For instance, two-dimensional (2D) second-order TIs with a quantized quadrupole moment, which is predicted by generalizing the fundamental relationship between the Berry phase and quantized polarization, support corner-localized modes lying in the middle of the energy gap¹⁷. Following the theoretical proposals of quadrupole TIs (QTIs), the topological corner states were observed experimentally in phononic^{18–20} and photonic^{21–26} systems.

The understanding of topological phases of matter has always been based on the topological band theory, which is defined in crystalline materials with long-range order and periodicity. To the best of our knowledge, topological phases are observed only in one-dimensional quasicrystals²⁷. Although there are predictions of topological phases in 2D quasicrystals^{28–43}, the experimental observations have never been reported.

Highly customizable electrical circuits have emerged as a new platform to engineer various topological states^{44–59}. In this study, we report the realization of the 2D quasicrystalline QTIs in electrical circuits and observe the corner states experimentally. To realize the QTIs, we construct the Ammann–Beenker (AB) tiling circuits with two types (thin and fat) of rhombuses and we implement the nearest- and next-nearest-neighbor hoppings using lumped elements to realize rotational symmetry. Using impedance measurement, the corner states protected by quantized quadrupole moment are directly observed in the circuits. The robustness of topological corner states is also demonstrated. Our work provides the experimental evidence of topological phases in 2D quasicrystalline systems. We expect more topological states can be observed in circuits based on similar implementations.

Results

Quasicrystalline QTIs. We construct the QTI on an AB tiling quasicrystal by only considering nearest- and next-nearest-neighbor hoppings³⁵. The tight-binding Hamiltonian is

$$H = A_0 \sum_j c_j^\dagger (\Gamma_2 + \Gamma_4) c_j + \frac{A_1}{2} \sum_{j \neq k} c_j^\dagger T(\phi_{jk}) c_k, \quad (1)$$

where

$$T(\phi_{jk}) = \begin{cases} \Gamma_4 - i\Gamma_3, & -\pi/4 \leq \phi_{jk} < \pi/4, \\ \Gamma_2 - i\Gamma_1, & \pi/4 \leq \phi_{jk} < 3\pi/4, \\ \Gamma_4 + i\Gamma_3, & 3\pi/4 \leq \phi_{jk} < 5\pi/4, \\ \Gamma_2 + i\Gamma_1, & 5\pi/4 \leq \phi_{jk} < 7\pi/4, \end{cases} \quad (2)$$

and ϕ_{jk} indicates the polar angle of bond between site j and k with respect to the horizontal direction. Here, $c_j^\dagger = (c_{j1}^\dagger, c_{j2}^\dagger, c_{j3}^\dagger, c_{j4}^\dagger)$ is the creation operator in cell j . The first and second terms are the intracell and intercell hoppings with amplitudes A_0 and A_1 , respectively. $\Gamma_4 = \tau_1 \tau_0$ and $\Gamma_\nu = -\tau_2 \tau_\nu$ with $\nu = 1, 2, 3$. $\tau_{1,2,3}$ are the Pauli matrices and τ_0 is the identity matrix. This model has a fourfold rotational symmetry $C_4 = UR$, where $U = \begin{pmatrix} 0 & i\tau_2 \\ \tau_0 & 0 \end{pmatrix}$ and R is an orthogonal matrix permuting the sites of the tiling to rotate the whole system by $\pi/4$.

The rotational symmetry C_4 results in a quantized quadrupole moment $Q_{xy} = 0, e/2$. Thus, Q_{xy} is a natural topological invariant,

which can be calculated in real space^{60,61}. By numerical calculations, we confirmed that the AB tiling quasicrystal has the non-trivial quadrupole moment $Q_{xy} = e/2$ under the hopping ratio $\lambda > 2.5 (\lambda = A_1/A_0)$ (see Supplementary Note 1). The quantized quadrupole moment indicates the occurrence of the quadrupole insulator with protected corner states.

Realization in electrical circuits. The quasicrystalline lattice can be mapped to an electrical circuit. To realize quasicrystalline QTI, we design an electrical circuit depicted in Fig. 1a. The circuit is characterized by the Kirchhoff's law

$$I_{pa} = \sum_{qb} J_{pa,qb}(\omega) V_{qb}(\omega), \quad (3)$$

where $I_{pa}(t) = I_{pa}(\omega) e^{i\omega t}$ [$V_{qb}(t) = V_{qb}(\omega) e^{i\omega t}$] is the current (voltage) at site $a(b)$ in cell $p(q)$ and ω is the frequency of the circuit. The circuit Laplacian is $J_{pa,qb}(\omega) = i\omega H_{pa,qb}(\omega)$, where

$$H_{pa,qb}(\omega) = C_{pa,qb} - \frac{1}{\omega^2} W_{pa,qb}, \quad (4)$$

with $C_{pa,qb}$ being the capacitance between two sites and $W_{pa,qb} = L_{pa,qb}^{-1}$ being the inverse inductivity between two sites. Here, the subscript g means the ground. $H_{pa,qb}$ can be equivalent to the Hamiltonian of quasicrystal in Eq. (1) if the diagonal elements are zero at ω_0 . For the diagonal components with $pa = qb$, the grounded elements are chosen for satisfying $C_{pa,pa} = -C_{pa,g} - \sum_{q'b'} C_{pa,q'b'}$ and $W_{pa,pa} = -L_{pa,g}^{-1} - \sum_{q'b'} L_{pa,q'b'}^{-1}$.

As shown in Fig. 1a, the solid and dashed lines correspond to hoppings with positive and negative values, which can be realized by the capacitors and inductors, respectively. We choose capacitor C_1 and inductor L_1 for intracell hopping, and C_2 and L_2 for intercell hopping. The nearest-neighbor couplings between cells are introduced to stabilize the corner states in small size systems³⁵. If these couplings are neglected, the exact AB tiling is restored and the physical results do not change qualitatively.

Under a suitable choice of the grounded elements, the tight-binding Hamiltonian of the QTI on a quasicrystalline lattice in Eq. (1) is mapped to the circuit Hamiltonian in Eq. (2). It is noteworthy that there exists a relation $C_2/C_1 = L_1/L_2 = A_1/A_0$.

The two-point impedance is:

$$Z_{ab} = \frac{V_a - V_b}{I_{ab}} = \sum_n \frac{|\psi_{n,a} - \psi_{n,b}|^2}{j_n} \quad (5)$$

where $V_{a(b)}$ is the voltage on site $a(b)$, I_{ab} is the current between the two sites, and j_n and $|\psi_n\rangle$ are the eigenvalue and eigenstates of the matrix $J(\omega)$, respectively²². The two-point impedance Z_{ab} diverges in the presence of zero-admittance modes ($j_n = 0$) with $\psi_{n,a} \neq \psi_{n,b}$. Hence, the corner states with zero-admittance can be observed by measuring the two-point impedance.

We consider the QTI on an AB tiling 2D quasicrystalline lattice. A circuit that realizes the QTIs is depicted in Fig. 1a. The unit cell of the circuit contains four sites denoted by labels 1, 2, 3, and 4. Each unit cell consists of three capacitors for positive coupling and one inductor for negative coupling, which can generate a synthetic magnetic π flux threading the unit-cell plaquette (equivalent to half the magnetic flux quantum, $(1/2)\Phi_0 = h/(2e)$, where h is the Planck constant). The existence of this non-zero flux opens the spectral gap for maintaining the corner-localized mid-gap modes. We use two pairs of capacitors and inductors (C_1, L_1) and (C_2, L_2), which have the same resonant frequency $\omega_0 = 1/\sqrt{L_1 C_1} = 1/\sqrt{L_2 C_2}$, as the intracell and intercell wirings between the sites, respectively. The intracell and intercell elements are related by $C_2 = \lambda C_1$ and $L_2 = L_1/\lambda$. The

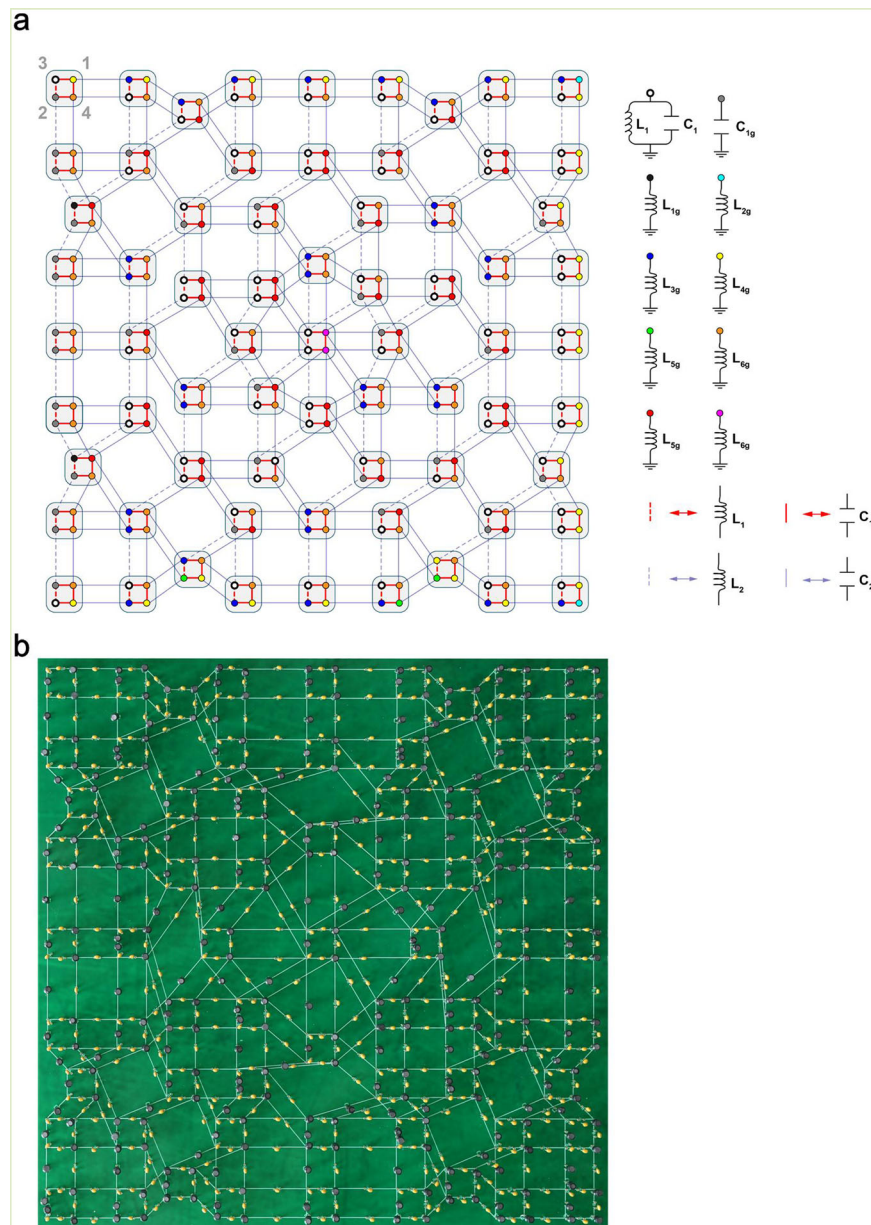


Fig. 1 Quasicrystalline quadrupole topological insulators in electrical circuits. **a** Schematic of the circuit with 69 unit cells. One unit cell consists of four sites labeled as 1, 2, 3, and 4 at the left-up corner. The colored sites are wired to grounded inductors and/or capacitors listed on the right. For example, the black hollow point 3 is connected to the ground by the capacitor–inductor pairs C_1 and L_1 , and the yellow point 1 is connected to the ground by L_{4g} . The sites in the same unit cell are wired by intracell inductors L_1 (red dashed lines) and capacitors C_1 (red solid lines), and the intercell elements between the unit cells are inductors L_2 (gray dashed lines) and capacitors C_2 (gray solid lines). **b** Photo of the fabricated circuit. The yellow and black elements are capacitors and inductors, respectively, and the wirings are indicated on overlay of the printed circuit board.

circuit is governed by the linear circuit theory with a circuit Laplacian $J(\omega)$ ²². The circuit has a square-open boundary, which satisfies the global C_4 symmetry at the resonant frequency ω_0 . Suitable grounded elements on the sites are chosen (site colors depicted in Fig. 1a indicate the values of the grounded capacitors and/or inductors) to sustain chiral symmetry at ω_0 , which pins the topological boundary modes in the middle of the bulk energy gap. The symmetry characteristic and quantized quadrupole moment of circuit indicate the occurrence of the QTI associated with topologically protected states localized on the corner sites. The edge states are gapped and merged with the bulk states. Hence, it is difficult to observe them experimentally (see Supplementary Note 2).

To realize the QTI experimentally, a circuit with 69 unit cells was fabricated as shown in Fig. 1b. The intracell elements with $C_1 = 10$ nF and $L_1 = 1$ mH result in a resonant frequency 50.3 kHz (parameters for other elements are given in “Methods”). Here we set the coupling ratio $\lambda = 10$, to get highly localized corner states, which can be observed by two-point impedance measurements between the corner/edge/bulk site and another bulk site using an impedance analyzer.

Figure 2 compares the experimental and theoretical results, which demonstrates the spectral and spatial localizations of the topological corner states. Figure 2a shows the spectrum of the circuit Laplacian $J(\omega)$ as a function of the normalized frequency ω/ω_0 . The isolated corner modes reside in the spectral gap of $J(\omega)$ at

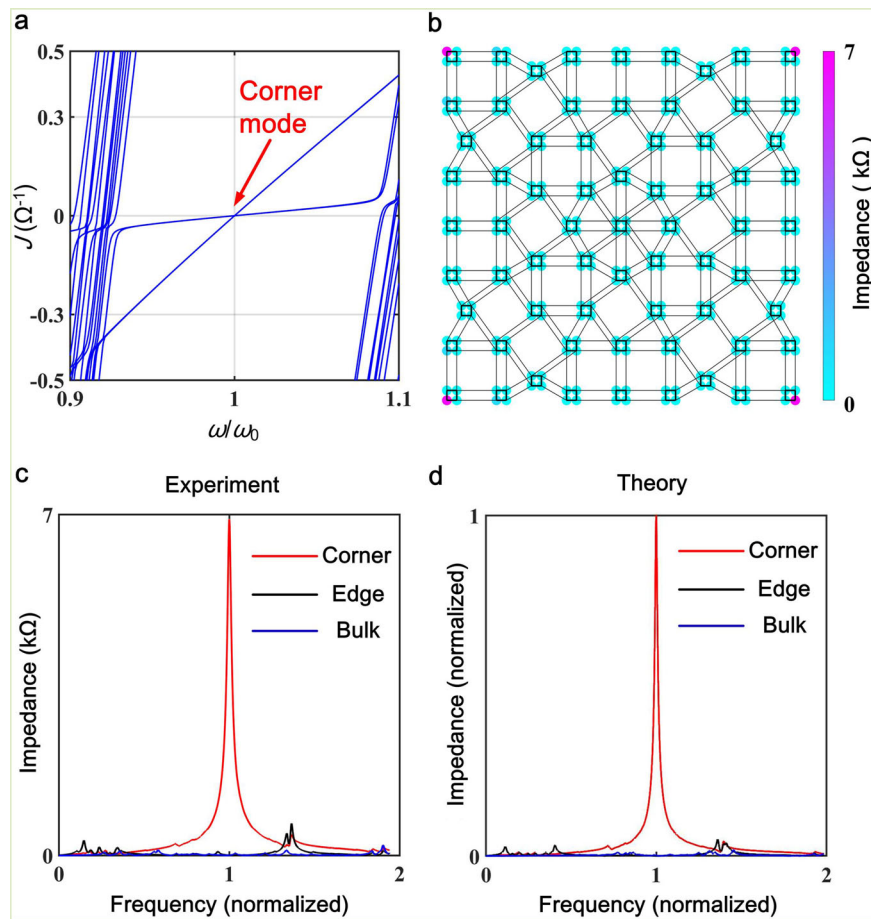


Fig. 2 Corner states on the circuit. **a** Spectra of the Laplacian J vs. the frequency that is normalized to the resonant frequency ω_0 . The isolated mode crossing in the gap corresponds to the topological corner states. **b** The experimental impedance distribution at the resonant frequency ω_0 demonstrates the spatial localization of the corner states. **c** The experimental two-point impedances measured between the left-up corner/edge/bulk site and another bulk site. **d** The theoretical two-point impedances. Both the experimental and theoretical results demonstrate the spectral localization of the corner states.

a fixed frequency ω_0 . The spatial distribution of the experimentally observed impedance of the corner states at ω_0 is illustrated in Fig. 2b. The impedance is maximum at the four corner sites and exponentially decays at other sites. The comparison between the experimental and theoretical impedance spectra is shown in Fig. 2c, d, which demonstrate the spectral localization of the corner modes. The maximum measured impedance reaches 7 k Ω .

To justify the robustness of the corner states, we consider the effect of experimental element errors. The errors are generated in two ways: (i) random manufacturing variations in discrete elements and (ii) the deviation of the typical values of commercially available circuit components from the theoretical circuit parameters. Figure 3a shows the normalized eigenfrequencies ω/ω_0 of the Laplacian $J(\omega)$ with element error $\pm 5\%$ and the number of the samples is 300. The eigenfrequencies of corner states (indicated by red circles) are located in the bandgap and far away from those of other states (indicated by blue circles). Experimentally, we construct a circuit with element error $\pm 5\%$ and measure the two-point impedances as a function of the normalized frequency ω/ω_0 . As shown in Fig. 3b, the corner states are spectrally localized with a deviation from ω_0 . Figure 3c–f shows the spatial impedance distributions at the frequencies of the four corner states. Compared with the spatial impedance distribution in Fig. 2b, although the maximum impedances are located at only one of the four corner sites, the topological corner states are still spatially localized. The spectral and spatial localizations imply the robustness of corner states on the circuit.

Discussion

The quadruple insulators were always realized on periodic systems with translational symmetry and the quadruple moments are well-defined in momentum space. Unlike the periodic structures, the quasi-periodic systems possess long-range order but do not have translational symmetry. Therefore, quasicrystalline insulators with a quantized quadrupole moment extend the concept of quadruple insulators defined in crystals. The realization of quadruple insulator in this work opens a way for the implementation of corner states in more quasi-periodic systems.

The circuit implementation of the 2D quasicrystalline QTIs confirms the existence and robustness of the corner states on the circuit. This work provides an experimental evidence for the first time to implement the topological phase in a 2D quasicrystalline system and extends the territory of topological phases beyond crystals to higher-dimensional aperiodic systems. The highly customizable circuit platform can also readily be applied to other 2D quasicrystals with different symmetries and to three-dimensional quasicrystalline structures⁶², which may realize more exotic topological states.

Methods

We choose the capacitors $C_1 = 10$ nF, $C_2 = 100$ nF, $C_{1g} = 100$ nF, $C_{2g} = 200$ nF, and the inductors $L_1 = 1000$ μ H, $L_2 = 100$ μ H with high Q factors ($Q > 70$ @ 50 kHz). The grounded elements are $L_{1g} = 83$ μ H, $L_{2g} = 100$ μ H, $L_{3g} = 45$ μ H, $L_{4g} = 31$ μ H, $L_{5g} = 23$ μ H, $L_{6g} = 500$ μ H, and $L_{7g} = 50$ μ H. After delicately choosing, the errors of the circuit elements are $< \pm 1\%$. The intracell elements C_1 and L_1 result in a resonant frequency 50.3 kHz. Here we set the coupling ratio $\lambda = 10$ in

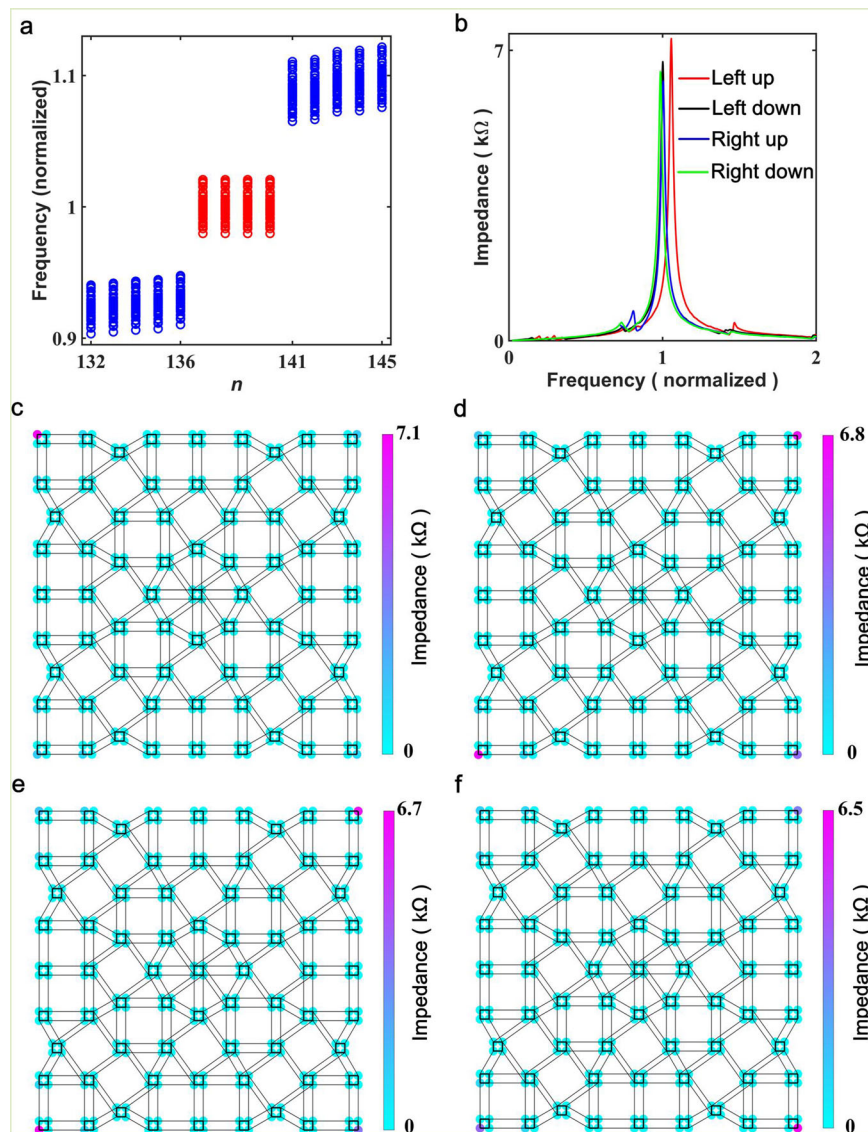


Fig. 3 Robustness of corner states on the circuit. **a** The normalized eigenfrequencies ω/ω_0 of the circuit Laplacian $J(\omega)$ with element errors $\pm 5\%$ and the number of the samples is 300. The eigenfrequencies of the corner and bulk states are indicated by the red and blue circles. **b** The experimental two-point impedances measured between the left-up/left-down/right-up/right-down corner site and another bulk site. **c-f** The experimental impedance distributions at the frequencies of the left-up/left-down/right-up/right-down corner states.

order to get highly localized corner states and the two-point impedance measurement is carried out using an Impedance Analyzer 4192A LF.

Data availability

The data that support the findings of this study are available from the corresponding author upon reasonable request.

Received: 18 December 2020; Accepted: 22 April 2021;

Published online: 26 May 2021

References

- Hasan, M. Z. & Kane, C. L. Topological insulators. *Rev. Mod. Phys.* **82**, 3045 (2010).
- Qi, X. L. & Zhang, S. Topological insulators and superconductors. *Rev. Mod. Phys.* **83**, 1057 (2011).
- Yang, Y. et al. Realization of a three-dimensional photonic topological insulator. *Nature* **565**, 622 (2019).
- Gao, W. et al. Topological photonic phase in chiral hyperbolic metamaterials. *Phys. Rev. Lett.* **114**, 037402 (2015).
- Jia, H. et al. Observation of chiral zero mode in inhomogeneous three-dimensional Weyl metamaterials. *Science* **363**, 148 (2019).
- Xue, H., Yang, Y., Gao, F., Chong, Y. & Zhang, B. Acoustic higher-order topological insulator on a kagome lattice. *Nat. Mater.* **18**, 108 (2019).
- Schindler, F. et al. Higher-order topology in bismuth. *Nat. Phys.* **14**, 918 (2018).
- Noh, J. et al. Topological protection of photonic mid-gap defect modes. *Nat. Photonics* **12**, 408 (2018).
- Xiang, N., Matthew, W., Alù, A. & Khanikaev, A. B. Observation of higher-order topological acoustic states protected by generalized chiral symmetry. *Nat. Mater.* **18**, 113 (2019).
- Li, M. et al. Higher-order topological states in photonic kagome crystals with long-range interactions. *Nat. Photonics* **14**, 89 (2020).
- Benalcazar, W. A., Bernevig, B. A. & Hughes, T. L. Quantized electric multipole insulators. *Science* **357**, 61 (2017).
- Slager, R. J., Rademaker, L., Zaenen, J. & Balents, L. Impurity-bound states and Green's function zeros as local signatures of topology. *Phys. Rev. B* **92**, 085126 (2015).
- Langbehn, J., Peng, Y., Trifunovic, L., Oppen, F. & Brouwer, P. W. Reflection-symmetric second-order topological insulators and superconductors. *Phys. Rev. Lett.* **119**, 246401 (2017).
- Song, Z., Fang, Z. & Fang, C. ($d-2$)-Dimensional edge states of rotation symmetry protected topological states. *Phys. Rev. Lett.* **119**, 246402 (2017).

15. Wladimir, A., Bernevig, B. A. & Hughes, T. L. Electric multipole moments, topological multipole moment pumping, and chiral hinge states in crystalline insulators. *Phys. Rev. B* **96**, 245115 (2017).
16. Schindler, F. et al. Higher-order topological insulators. *Sci. Adv.* **4**, eaat0346 (2018).
17. Peterson, C. W., Benalcazar, W. A., Hughes, T. L. & Bahl, G. Quantized microwave quadrupole insulator with topologically protected corner states. *Nature* **555**, 346 (2018).
18. Serra-Garcia, M. et al. Observation of a phononic quadrupole topological insulator. *Nature* **555**, 342 (2018).
19. Xue, H. et al. Observation of an acoustic octupole topological insulator. *Nat. Commun.* **11**, 2442 (2020).
20. Ni, X., Li, M., Weiner, M., Alù, A. & Khanikaev, A. B. Demonstration of a quantized acoustic octupole topological insulator. *Nat. Commun.* **11**, 2108 (2020).
21. Xie, B. Y. et al. Second-order photonic topological insulator with corner states. *Phys. Rev. B* **98**, 205147 (2018).
22. Imhof, S. et al. Topoelectrical-circuit realization of topological corner modes. *Nat. Phys.* **14**, 925 (2018).
23. Bao, J. et al. Topoelectrical-circuit octupole insulator with topologically protected corner states. *Phys. Rev. B* **100**, 201406(R) (2019).
24. Zhang, X. et al. Symmetry-protected hierarchy of anomalous multipole topological band gaps in nonsymmorphic metacrystals. *Nat. Commun.* **11**, 65 (2020).
25. Mittal, S. et al. Photonic quadrupole topological phases. *Nat. Photonics* **13**, 692 (2019).
26. He, L., Addison, Z., Mele, E. & Zhen, B. Quadrupole topological photonic crystals. *Nat. Commun.* **11**, 3119 (2020).
27. Kraus, Y., Lahini, Y., Ringel, Z., Verbin, M. & Zilberberg, O. Topological states and adiabatic pumping in quasicrystals. *Phys. Rev. Lett.* **109**, 106402 (2012).
28. Verbin, M., Zilberberg, O., Kraus, Y., Lahini, Y. & Silberberg, Y. Observation of topological phase transitions in photonic quasicrystals. *Phys. Rev. Lett.* **110**, 076403 (2013).
29. Kraus, Y., Ringel, Z. & Zilberberg, O. Four-dimensional quantum Hall effect in a two-dimensional quasicrystal. *Phys. Rev. Lett.* **111**, 226401 (2013).
30. Kraus, Y. & Zilberberg, O. Quasiperiodicity and topology transcend dimensions. *Nat. Phys.* **12**, 624 (2016).
31. Tran, D., Dauphin, A., Goldman, N. & Gaspard, P. Topological Hofstadter insulators in a two-dimensional quasicrystal. *Phys. Rev. B* **91**, 085125 (2015).
32. Bandres, M. A., Rechtsman, M. C. & Segev, M. Topological photonic quasicrystals: fractal topological spectrum and protected transport. *Phys. Rev. X* **6**, 011016 (2016).
33. Fulg, I. C., Pikulin, D. I. & Loring, T. A. Aperiodic weak topological superconductors. *Rhevs. Rev. Lett.* **116**, 257002 (2016).
34. Huang, H. & Liu, F. Quantum spin Hall effect and spin Bott Index in a quasicrystal lattice. *Phys. Rev. Lett.* **121**, 126401 (2018).
35. Chen, R., Chen, C., Gao, J., Zhou, B. & Xu, D. Higher-order topological insulators in quasicrystals. *Phys. Rev. Lett.* **124**, 036803 (2020).
36. Hua, C., Chen, R., Zhou, B. & Xu, D. Higher-order topological insulator in a dodecagonal quasicrystal. *Phys. Rev. B* **102**, 241102 (2020).
37. Varjas, D. et al. Topological phases without crystalline counterparts. *Phys. Rev. Lett.* **123**, 196401 (2019).
38. Chen, R., Xu, D. & Zhou, B. Topological Anderson insulator phase in a quasicrystal lattice. *Phys. Rev. B* **100**, 115311 (2019).
39. Longhi, S. Topological phase transition in non-Hermitian quasicrystals. *Phys. Rev. Lett.* **112**, 237601 (2019).
40. Vidal, J. & Mosseri, R. Quasiperiodic tilings in a magnetic field. *J. Non-Cryst. Solids* **334**, 130-136 (2004).
41. Fuchs, J. N. & Vidal, J. Hofstadter butterfly of a quasicrystal. *Phys. Rev. B* **94**, 205437 (2016).
42. Fuchs, J. N., Mosseri, R. & Vidal, J. Landau levels in quasicrystals. *Phys. Rev. B* **98**, 165427 (2018).
43. Adhip Agarwala, Vladimir Juričić & Bitan Roy. Higher-order topological insulators in amorphous solids. *Phys. Rev. Res.* **2**, 1 (2020)
44. Luo, K., Yu, R. & Weng, H. Topological nodal states in circuit lattice. *Research* **2018**, 6793752 (2018).
45. Yu, R., Zhao, Y. X. & Schnyder, A. P. A genuine realization of the spinless 4D topological insulator by electric circuits. *Nat. Sci. Rev.* **7**, 1288 (2020).
46. Lee, C. H. et al. Topoelectrical circuits. *Commun. Phys.* **1**, 39 (2018).
47. Ezawa, M. Higher-order topological electric circuits and topological corner resonance on the breathing kagome and pyrochlore lattices. *Phys. Rev. B* **98**, 201402(R) (2018).
48. Serra-Garcia, M., Süssstrunk, R. & Huber, S. D. Observation of quadrupole transitions and edge mode topology in an LC circuit network. *Phys. Rev. B* **99**, 020304(R) (2019).
49. Helbig, T. et al. Band structure engineering and reconstruction in electric circuit networks. *Phys. Rev. B* **99**, 161114(R) (2019).
50. Lu, Y. et al. Probing the Berry curvature and Fermi arcs of a Weyl circuit. *Phys. Rev. B* **99**, 020302(R) (2019).
51. Zangeneh-Nejad, F. & Fleury, R. Nonlinear second-order topological insulators. *Phys. Rev. Lett.* **123**, 053902 (2019).
52. Bao, J. et al. Topoelectrical circuit octupole insulator with topologically protected corner states. *Phys. Rev. B* **100**, 201406(R) (2019).
53. Yang, H., Li, Z.-X., Liu, Y., Cao, Y. & Yan, P. Observation of symmetry-protected zero modes in topoelectrical circuits. *Phys. Rev. Res.* **2**, 022028(R) (2020).
54. Zhang, W. et al. Topoelectrical-circuit realization of 4D hexadecapole insulator. *Phys. Rev. B* **102**, 100102(R) (2020).
55. Ningyuan, J., Owens, C., Sommer, A., Schuster, D. & Simon, J. Time- and site-resolved dynamics in a topological circuit. *Phys. Rev. X* **5**, 021031 (2015).
56. Albert, V. V., Glazman, L. I. & Jiang, L. Topological properties of linear circuit lattices. *Phys. Rev. Lett.* **114**, 173902 (2015).
57. Li, R. et al. Ideal type-II Weyl points in topological circuits. *Nat. Sci. Rev.* **nwa192** (2020).
58. Dong, J., Juričić, V. & Roy, B. Topoelectric circuits: Theory and construction. *Phys. Rev. Res.* **3**, 023056 (2021).
59. Zhang, Z. Q., Wu, B. L., Song, J. & Jiang, H. Topological Anderson insulator in electric circuits. *Phys. Rev. B* **100**, 184202 (2019).
60. Ono, S., Trifunovic, L. & Watanabe, H. Difficulties in operator-based formulation of the bulk quadrupole moment. *Phys. Rev. B* **100**, 245133 (2019).
61. Kang, B., Shiozaki, K. & Cho, G. Y. Many-body order parameters for multipoles in solids. *Phys. Rev. B* **100**, 245134 (2019).
62. Jeon, S., Kwon, H. & Hur, K. Intrinsic photonic wave localization in a three-dimensional icosahedral quasicrystal. *Nat. Phys.* **13**, 363 (2017).

Acknowledgements

B.L. was sponsored by the Fundamental Research Funds for the Central Universities under Grant numbers 3072020CFT2501 and 3072020CF2528, and the National Natural Science Foundation of China under Grant number 61901133. R.C. acknowledges support from the project funded by the China Postdoctoral Science Foundation (Grant number 2019M661678). J.S. was sponsored by the National Natural Science Foundation of China under Grant numbers 91750107 and 61875044. D.-H.X. was supported by the NSFC (Grant number 12074108 and 11704106). D.-H.X. also acknowledges the financial support of the Chutian Scholars Program in Hubei Province.

Author contributions

B.L., R.C., and R.L. conceived the idea and carried out the calculations. B.L. and H.T. processed the experimental data. B.L., R.L., H.T., G.D., C.Z., Y.L., and Y.W. designed the experimental setup and made the measurements. B.L. and R.L. wrote the manuscript with input from all authors. R.L., H.T., C.G., B.Z., J.S., and D.-H.X. supervised the project.

Competing interests

The authors declare no competing interests.

Additional information

Supplementary information The online version contains supplementary material available at <https://doi.org/10.1038/s42005-021-00610-7>.

Correspondence and requests for materials should be addressed to R.L., H.T., J.S. or D.-H.X.

Reprints and permission information is available at <http://www.nature.com/reprints>

Publisher's note Springer Nature remains neutral with regard to jurisdictional claims in published maps and institutional affiliations.



Open Access This article is licensed under a Creative Commons Attribution 4.0 International License, which permits use, sharing, adaptation, distribution and reproduction in any medium or format, as long as you give appropriate credit to the original author(s) and the source, provide a link to the Creative Commons license, and indicate if changes were made. The images or other third party material in this article are included in the article's Creative Commons license, unless indicated otherwise in a credit line to the material. If material is not included in the article's Creative Commons license and your intended use is not permitted by statutory regulation or exceeds the permitted use, you will need to obtain permission directly from the copyright holder. To view a copy of this license, visit <http://creativecommons.org/licenses/by/4.0/>.

© The Author(s) 2021, corrected publication 2021